0022-3565/11/3363-716–723
THE JOURNAL OF PHARMACOLOGY AND EXPERIMENTAL THERAPEUTICS
U.S. Government work not protected by U.S. copyright
JPET 336:716–723, 2011

Vol. 336, No. 3
173609/3670837
Printed in U.S.A.

Pharmacokinetic Modeling and [^{123}I]5-IA-85380 Single Photon Emission Computed Tomography Imaging in Baboons: Optimization of Dosing Regimen for ABT-089

Chih-Liang Chin, Robert A. Carr, Daniel A. Llano, Olivier Barret, Hongyu Xu, Jeffrey Batis, Andrei O. Koren, John P. Seibyl, Kennan C. Marsh, Gilles Tamagnan, Michael W. Decker, Mark Day, and Gerard B. Fox

Advanced Technology (C.-L.C., M.D., G.B.F.), Exploratory Science (R.A.C., H.X., K.C.M.), Neuroscience Development (D.A.L.), Neuroscience Discovery (M.W.D.), Global Pharmaceutical Research and Development, Abbott Laboratories, Abbott Park, Illinois; Molecular NeuroImaging, L.L.C., New Haven, Connecticut; (O.B., J.B., A.O.K., J.P.S., G.T.), and Department of Psychiatry, Yale University School of Medicine and Veterans Affairs Connecticut Healthcare System, West Haven, Connecticut (J.P.S., G.T.)

Received August 16, 2010; accepted December 14, 2010

ABSTRACT

Neuronal acetylcholine nicotinic receptors (nAChRs) are targets for the development of novel treatments of brain diseases. However, adverse effects (for example, emesis or nausea) associated with high drug maximal exposures or C_{max} at nAChRs often hinder the advancement of experimental compounds in clinical trials. Therefore, it is essential to explore the feasibility of maintaining exposures below a predetermined C_{max} while sustaining targeted CNS effects. By use of a [^{123}I]5-IA [5-[^{123}I]iodo-3-[2(*S*)-azetidinylmethoxy]pyridine] displacement SPECT imaging paradigm in nonhuman primates, we compared brain nAChR binding activity elicited by either a bolus injection or by slow infusion of an identical dose of a novel neuronal nicotinic agonist, ABT-089 [2-methyl-3-(2-(*S*)-pyrrolidinylmethoxy)pyridine dihydrochloride], where the slow infusion scheme was derived from a two-compartment pharmacokinetic modeling designed to limit the C_{max}. We determined [^{123}I]5-IA displacement using doses of ABT-089 (0.04, 0.4, and 1.0 mg/kg i.v.) that encompassed efficacious drug exposures in nonhuman primates and examined the relationship between ABT-089 displacement ratios and plasma exposures. Our results indicated that calculated displacement ratios were quite similar between the two different dosing regimens despite substantial differences in C_{max}. In addition, displacement ratios correlated well with drug exposures calculated as the area-under-curve (AUC) of plasma concentration and varied in a dose-dependent manner, suggesting that displacement ratios are driven by the AUC of drug plasma exposure but not C_{max}. Our data demonstrate the feasibility of predicting plasma exposures using a two-compartment pharmacokinetic model and its potential for optimizing dosing regimens.

Introduction

Nicotinic acetylcholine receptors (nAChRs) are excitatory, acetylcholine-gated cation channels that are widely distributed in the central and peripheral nervous systems (Paterson and Nordberg, 2000). nAChRs can be assembled from a range of subunits (α_2–α_{10}; β_2–β_4), in which two of the most abundant nAChR subtypes found in the brain are α_7 and $\alpha_4\beta_2$* receptors (Gotti and Clementi, 2004). Investigations of the nicotinic cholinergic system have demonstrated that dysfunction of nAChRs can contribute to a wide spectrum of neurological and psychiatric disorders, including attention deficit hyperactivity disorder, schizophrenia, and Alzheimer's and Parkinson's diseases (Hogg and Bertrand, 2007). As a result, nAChRs have become attractive therapeutic targets for developing novel treatments for these devastating diseases (Decker et al., 2001). However, addiction liability associated with nicotinic compounds and their adverse effect profiles,

This work was supported in part by Abbott Laboratories.
Article, publication date, and citation information can be found at http://jpet.aspetjournals.org.
doi:10.1124/jpet.110.173609.

ABBREVIATIONS: nAChR, neuronal acetylcholine nicotinic receptor; AUC, area under the curve; CNS, central nervous system; ABT-089, 2-methyl-3-(2-(*S*)-pyrrolidinylmethoxy)pyridine dihydrochloride; PET, positron emission tomography; SPECT, single photon emission computed tomography; PK, pharmacokinetic; $C_{max,}$, maximal plasma exposure; CL systemic clearance; V_c, volume of distribution of plasma; V_t, volume of distribution of tissue; CL_d, intercompartmental clearance; VOI, volume of interest; f_P, free plasma concentration; V_T, volume of distribution; HPLC, high-performance liquid chromatography; A-85380, 3-[2(*S*)-2-azetidinylmethoxy]pyridine; TAC, time-activity curve; 5-IA, 5-iodo-3-[2(*S*)-azetidinylmethoxy]pyridine.

particularly increased incidence of emesis at higher exposures, have imposed significant hurdles to further clinical development of therapeutic agents acting at nAChRs (Beleslin and Krstić, 1987; Faessel et al., 2006; Hogg and Bertrand, 2007).

Radiotracer imaging techniques, such as positron emission tomography (PET) and single photon emission computed tomography (SPECT), have been applied to facilitate CNS drug discovery and development at various stages (Frank and Hargreaves, 2003; Fox et al., 2009; Wong et al., 2009), such as target validation or early proof-of-concept clinical studies. Significant advances in neuroreceptor or transport imaging have offered great insights into brain functions, allowing characterization of receptor density or neurotransmitter systems in normal as well as diseased conditions (Frankle and Laruelle, 2002; Zipursky et al., 2007; Howell, 2008). Specifically, PET/SPECT imaging has been increasingly exploited for dose selection or patient stratification in clinical studies of novel CNS treatments (Wong et al., 2009). To visualize nAChRs binding activity, several radiolabeled analogs of the high-affinity nicotinic ligand A-85380 [3-[2(*S*)-2-azetidinylmethoxy]pyridine] (Sullivan et al., 1996) have been developed as SPECT tracers (Koren et al., 1998; Musachio et al., 1999; Zoghbi et al., 2001). In particular, 5-[^{123}I]iodo-3-[2(*S*)-azetidinylmethoxy]pyridine ([^{123}I]5-IA) has been extensively used as a SPECT radioligand for nAChRs. As shown by Fujita et al. (2003a), [^{123}I]5-IA rapidly penetrates the blood-brain barrier with low nonspecific binding and minimal toxicity. In addition, the same authors have also found that [^{123}I]5-IA seems to predominantly label the $\alpha_4\beta_2$* subtype and that radioligand uptake can be displaced by endogenous acetylcholine as well as by nicotine and cytisine (Fujita et al., 2003a).

ABT-089 [2-methyl-3-(2-(*S*)-pyrrolidinylmethoxy)pyridine dihydrochloride] is a selective partial agonist at nAChRs that has shown cognitive-enhancing properties in preclinical models of learning and memory (Decker et al., 1997) and, in some studies, in patients with adult attention deficit hyperactivity disorder (Wilens et al., 2006). Similar to other partial agonists, ABT-089 demonstrated a more advantageous safety profile in preclinical species than full agonists (Rueter et al., 2004), consistent with the notion of an increased safety margin of partial agonists relative to full agonists (Hogg and Bertrand, 2007). However, nicotinic compounds may require high doses to achieve clinical efficacy that, unfortunately, elevates the potential for adverse effects. In this study, by use of a [^{123}I]5-IA displacement imaging paradigm (Fujita et al., 2000), we sought to investigate an association for ABT-089 displacement ratios with its pharmacokinetic (PK) parameters (C_{max} and AUC) in baboons. We hypothesized that a slow infusion dosing regimen of ABT-089 could produce a lower C_{max} but still achieve displacement ratios similar to those of a bolus injection. Toward this goal, we first measured displacement ratios and plasma exposures in baboons injected with a bolus of ABT-089 at a dose of 0.4 mg/kg i.v. PK simulations then were performed to devise a dosing scheme constrained by a predetermined C_{max} value, and a corresponding imaging experiment was conducted. Afterward, the studies were repeated at different doses of ABT-089 (0.04 and 1 mg/kg i.v.) to delineate the full dose response. Finally, the relationship between displacements ratios and calculated C_{max} or AUC was determined.

Materials and Methods

Animals and Drug Preparation. All experiments were conducted in accordance with Institutional Animal Care and Use Committee (IACUC) guidelines at the VA Medical Center (West Haven, CT) and were reviewed and approved by the IACUC at Abbott Laboratories. Facilities at the VA Medical Center are further accredited by the Association for the Assessment and Accreditation of Laboratory Animal Care (AAALAC). Ovariectomized female baboons (*Papio anubis*) (n = 4, age ranged from 6 to 20 years of age) were used as research subjects (10 scans). ABT-089 (Decker et al., 1997) was synthesized at Abbott Laboratories and dissolved in sterile water. The drug was administered intravenously with either a bolus injection or a 24-min slow infusion determined by pharmacokinetic simulations. No-carrier-added sodium [^{123}I]iodide in 0.1 N NaOH (radionuclidic purity = 99.8%) was obtained from MDS Nordion (Vancouver, BC, Canada). Other reagents were of analytical grade and obtained from conventional chemical suppliers. Finally, 5-IA standard and precursor were prepared in-house following the published procedure (Musachio et al., 1999).

Radiochemistry and Metabolite Measurements. [^{123}I]5-IA was prepared using a modification of a previously published procedure (Horti et al., 1999). In brief, the following components were added to a vial with dry Na[^{123}I]I/NaOH: 125 μl of 75% acetic acid and 25% water, 100 μg of *N-tert*-butoxycarbonyl-protected trimethylstannyl precursor (Koren et al., 1998) in 50 μl of methanol, and 125 μl of a 5 mg/ml solution of chloramine-T in methanol. The reaction mixture was heated at 100°C for 14 to 16 min, cooled for 4 to 6 min in ice-cold water, and quenched by the addition of 100 μl of a 100 mg/ml aqueous solution of $Na_2S_2O_5$. The vial headspace was flushed with 10 ml of air into a charcoal filter, and then the quenched reaction mixture was injected onto a reverse-phase HPLC column, and the vial was rinsed with 0.2 to 0.3 ml of 50% aqueous acetonitrile and also injected into reverse-phase HPLC column. The column (Nova-Pak C18, 4 μm, 4.6 × 250 mm; Waters, Milford, MA) was eluted with a mixture of acetonitrile and water [67:33 (v/v)] at a flow rate of 1.0 ml/min. The fraction containing the radiolabeled *N-tert*-butoxycarbonyl-protected intermediate was collected into a 50-ml flask preloaded with 1 ml of trifluoroacetic acid, and the solvents were removed on a rotary evaporator at 40-45°C under reduced pressure and argon gas flow. The dry residue in the flask was treated with a mixture of 1 ml of trifluoroacetic acid and 4 ml of dichloromethane for 5 to 7 min at room temperature. Afterward, the content of the flask was evaporated to dryness (rotary evaporator, 40-45°C, reduced pressure, argon gas flow), reconstituted in 2 × 0.5 ml of 10% aqueous acetonitrile, and injected onto a reverse-phase HPLC column for final purification. The column (Gemini C18, 5 μm,, 4.6 × 250 mm; Phenomenex, Torrance, CA) was eluted with a mixture of acetonitrile, water, and trifluoroacetic acid [10:90:0.2 (v/v/v)] at a flow rate of 1.0 ml/min. The final product fraction was collected into a 50-ml flask, and the solvents were removed on a rotary evaporator at 40-45°C under reduced pressure and argon gas flow. The dry residue in the flask was dissolved in 0.4 ml of ethanol followed by 6 to 6.5 ml of sterile 0.9% sodium chloride for injection. The resulting solution was filtered through a 0.2-μm sterilizing filter into a sterile empty vial. Quality control testing included visual inspection, determination of radioactivity concentration, identity, and radiochemical purity by HPLC as well as pH, pyrogen content, and sterility. Decay-corrected production yield was in the range of 12 to 50%. Each synthesis produced tracers with high specific activity (>5000 Ci/mmol) and radiochemical purity (>95%). Finally, concentrations of parent [^{123}I]5-IA and its metabolite in the plasma as well as free faction were measured using venous blood samples as described previously by Zoghbi et al. (2001).

Pharmacokinetic Calculations and Simulations. Calculations and simulations were run on a Dell OptiPlex GX620 with 2.0 Gb of RAM and a 2.8-GHz Intel processor running on Microsoft Windows XP Professional and WinNonlin Professional, version 5.2.1

(Pharsight Corporation, St. Louis, MO). Pharmacokinetic parameters (C_{max} and $AUC_{0-\infty}$) were determined by fitting a two-compartment model (Gabrielsson and Weiner, 1999) using plasma exposure data obtained from each subject. The selection of two-compartment model, instead of a one-compartment model, was based on the Akaike Information Criterion, a measure of goodness of fit (Ludden et al., 1994), as well as visual inspection of the measured versus predicted concentration-time profiles. A schematic diagram of the two-compartment model is shown below where the model was parameterized in terms of total clearance (CL) and distribution clearance (CL_d) and central (V_c) and tissue (V_t) volume of distribution. As a basis for initial dosing regimen prediction, ABT-089 pharmacokinetics previously determined in cynomolgus monkeys (V_c = 2 l/kg, V_t = 3 l/kg, CL = 1.9 $l \cdot h^{-1} \cdot kg^{-1}$, CL_d = 3.5 $l \cdot h^{-1} \cdot kg^{-1}$) were assumed to be predictive of those in baboon (Scheme 1).

Using this model, simulated intravenous infusions to baboon of various doses and infusion durations were performed to determine the dosing regimen that would best approximate the optimally efficacious ABT-089 plasma concentration-time profile in rhesus monkeys (Decker et al., 1997). In addition to C_{max} and $AUC_{0-\infty}$, area under the plasma concentration-time curve was determined from the time of the start of the dose infusion to 100 min (1.67 h, $AUC_{0\text{-}1.67\ h}$) because maximal displacement (receptor occupancy) was observed at or near the 100-min time point.

[^{123}I]5-IA SPECT Imaging. All scans were acquired at Molecular NeuroImaging L.L.C. (New Haven, CT) on the NeuroFocus SPECT camera (NeuroLogica, Danvers, MA), a research-dedicated brain-imaging camera with an isotropic spatial resolution of approximately 2.5 to 3.5 mm. Four ovariectomized female baboons (16–17 kg) were used for the study. Animals were fasted for 18 to 24 h before imaging. On the day of imaging, the baboon was first anesthetized with intramuscular ketamine (10 mg/kg) and glycopyrrolate (0.01 mg/kg), transferred to the SPECT camera, and immediately intubated with an endotracheal tube for continued anesthesia with 2.5% isoflurane administered through a rebreathing circuit. An intravenous perfusion line was established in a leg vein for injection of fluids for hydration and collection of blood samples for metabolite analysis. Furthermore, a second line was established in the other leg for injection of the radiotracer. It is noteworthy that the interval between ketamine administration and the injection of [^{123}I]5-IA was at a minimum of 2 h to allow the physiology of the animal to stabilize under anesthesia. The subject's head was immobilized within the gantry with a "bean bag" that hardens upon evacuation of air (Olympic Medical, Seattle, WA). Body temperature was kept between 36.1 and 38.5°C using a heated water blanket, and vital signs, including heart rate, respiration rate, oxygen saturation, and body temperature, were monitored every 15 min during the study. The acquisition time for each data point was approximately 22 min, and the total imaging time was approximately 6 h.

Pharmacokinetic Analysis of ABT-089 Exposures. Plasma samples were collected and immediately stored in a freezer for later analysis. Samples were shipped from Molecular NeuroImaging L.L.C. to Abbott Laboratories and analyzed for concentrations of ABT-089. In brief, ABT-089 was selectively removed from plasma using protein precipitation with a mixture of acetonitrile and methanol [4:1 (v/v)]. Samples then were vortexed vigorously followed by centrifugation. The supernatant was transferred and evaporated to dryness with a gentle stream of nitrogen under gentle heat (approximately 35°C). Afterward, samples were reconstituted by vortexing with mobile phase. ABT-089 and its internal standard were separated from coextracted contaminants on a 50 × 3-mm Thermo Betasil CN column with an acetonitrile/ammonium acetate (10 mM) [16:84 (v/v)] mobile phase at a flow rate of 0.4 ml/min with a 10-μl injection. Finally, ABT-089 was quantified using multiple reaction monitor detection with a turbo ionspray source on a mass spectrometer (Applied Biosystems, Foster City, CA).

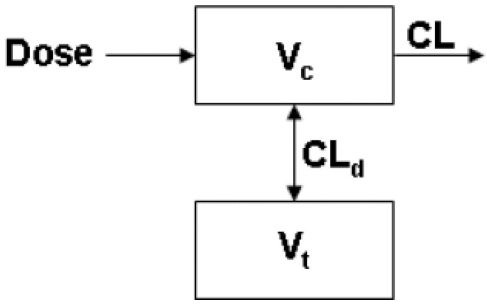

Scheme 1. A two-compartment model used for pharmacokinetic simulations.

Data Analysis. Raw data were reconstructed using an iterative three-dimensional algorithm provided by the manufacturer in which spatial filtering, noise reduction, and uniform attenuation correction (μ_{eff} = 0.012 mm^{-1}) were applied. Once reconstructed, image data were coregistered to a standard imaging template using statistical parametric mapping (Welcome Department of Cognitive Neurology, London, UK). Afterward, a radioligand-specific volume of interest (VOI) template was applied using multimodality radiological image processing (MEDx; Sensor System, Sterling, VA), in which each image volume (thalamus, frontal and parietal cortices, and cerebellum) was identified in the dynamic SPECT dataset. Total counts within the VOI, total volume of VOI, and count density (counts/voxel) were determined for each region from individual subjects. Accordingly, time-activity curves (TACs) were generated from VOIs, depicting the regional brain count density, reflecting total uptake. These TACs then were corrected for radioactive decay, and a calibration factor obtained from phantom studies was applied. Finally, the volume of distribution (V_T) of each VOI was derived and normalized by the concentration of the free [^{123}I]5-IA parent compound in plasma (f_P) at each time point. In the past, we have used and validated V_T/f_P as a suitable measure for nAChR binding activity because of the absence of a receptor-poor reference region (Fujita et al., 2000). Thus, calculations of the displacement were determined by taking the mean of the three images before either ABT-089 injection as a baseline, $(V_T/f_P)_{baseline}$, and subtracting the postdisplacing dose nadir, $(V_T/f_P)_{nadir}$, and then expressing this delta as percentage of baseline as follows: percentage displacement [%] = $([(V_T/f_P)_{baseline} - (V_T/f_P)_{nadir}] \times 100)/(V_T/f_P)_{baseline}$.

Results

Figure 1 illustrates the TACs obtained from a baboon administered with ABT-089 at 0.4 mg/kg via a bolus injection (Fig. 1A) or slow infusion (Fig. 1B). These data indicate that, regardless of the dosing regimen used, the highest uptake of [^{123}I]5-IA was found in thalamus with moderate binding in frontal and parietal cortices, whereas minimal activity was shown in cerebellum. These distributions are consistent with results reported from previous in vivo studies (Chefer et al., 1998; Fujita et al., 2000). Furthermore, considering regional differences in the rate of changes in activities before and after the ABT-089 injection (Fig. 1), the displacement by ABT-089 showed greater effect in thalamus (high nAChR density) than cerebellum (low nAChR density), suggesting that displacement resulted from specific nAChR binding and not from nonspecific binding. [^{123}I]5-IA has been validated and commonly used for imaging nAChRs in vivo across species in which the highest uptake of [^{123}I]5-IA in brain was consistently found in thalamus and with moderate cortical binding in rodents (Fox et al., 2009), primates (Baldwin et al., 2006), and human (Fujita et al., 2003b).

Corresponding measured and simulated PK data are shown in Fig. 2 where the kinetics of plasma exposures seem to be well described using a two-component model. A lower

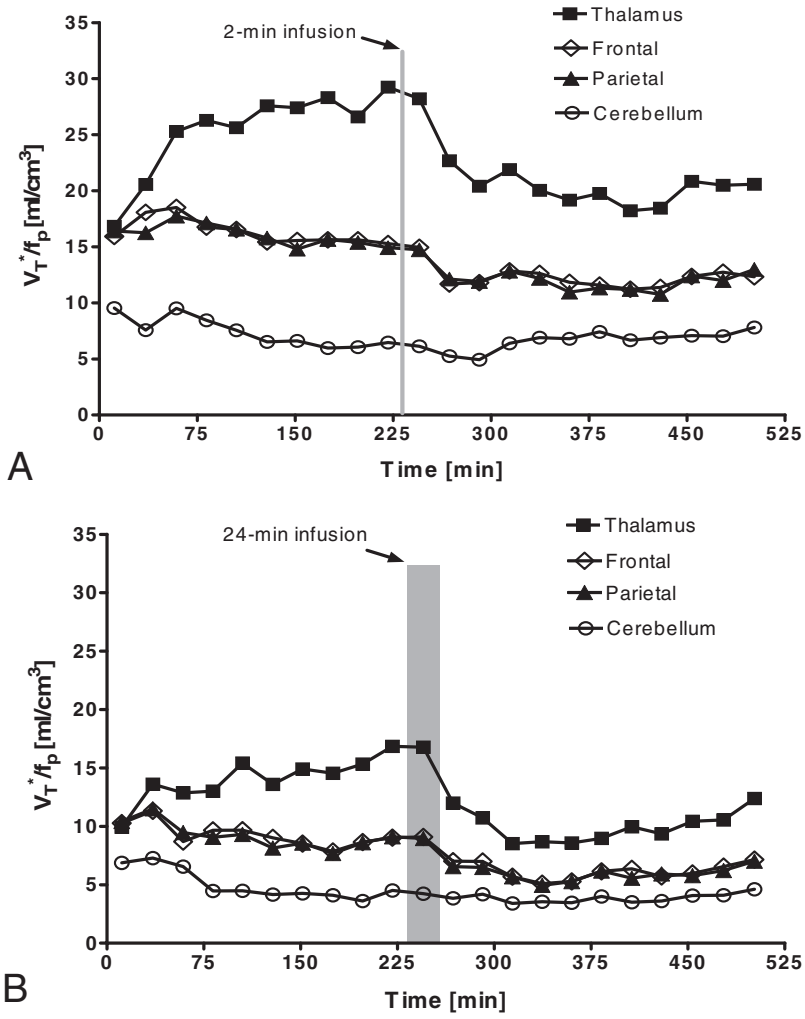

Fig. 1. The regional time-activity curves obtained from the baboons intravenously infused with ABT-089 at 0.4 mg/kg via a bolus injection (A) or slow infusion (B) The observed rank order of regional [^{123}I]5-IA uptake was thalamus > frontal and parietal cortices > cerebellum, which is consistent between two different dosing regimens.

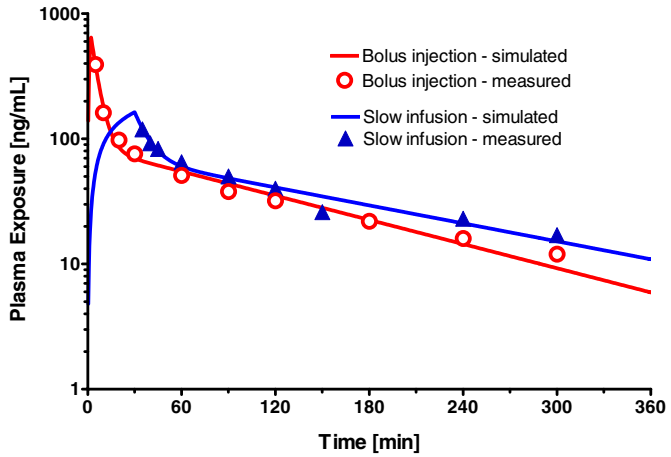

Fig. 2. Measured and simulated plasma exposures obtained from the baboons shown in Fig. 1. Compared with the bolus injection study of ABT-089 at the same dose (Fig. 1A), a substantially lower C_{max} value was achieved using slow infusion; however, the calculated displacement ratio was fairly in good agreement. In addition, pharmacokinetic analyses revealed that the measured plasma exposures can be simulated using a two-compartment model.

C_{max} was achieved when ABT-089 was given by slow infusion. Furthermore, our data show that ABT-089 displaced [^{123}I]5-IA binding more rapidly when the drug was given by a bolus injection, which can be associated with kinetics of drug exposures. Images of [^{123}I]5-IA uptake acquired at baseline and after ABT-089 infusion at various doses (0.01, 0.4, and 1 mg/kg i.v., slow infusion) are shown in Fig. 3, whereas the measured and simulated kinetics of ABT-089 exposures from each dosing group are shown in Fig. 4. It is evident that the binding activity in the thalamus was significantly diminished at the higher doses of ABT-089 and varied in a dose-related fashion. Table 1 lists plasma PK parameters (C_{max}, $AUC_{0\text{-}\infty}$, and $AUC_{0\text{-}1.67\ h}$) calculated from each subject as well as corresponding displacement ratios in which ABT-089 pharmacokinetics in baboon (V_c = 1.7 l/kg, V_t = 2.6 l/kg, CL = 1.6 l · h^{-1} · kg^{-1}, CL_d = 4.0 l · h^{-1} · kg^{-1}) were similar to those previously observed in cynomolgus monkeys. Consistent with imaging data, a dose response was observed from the calculated displacement ratios. It is remarkable that there is a good agreement in displacement ratios (mean ± S.E.M.) when 0.4 mg/kg ABT-089 was given via a bolus injection (42 ± 5.7%) or by slow infusion (38 ± 5.6%), even though the observed C_{max} values are substantially different (see Table 1 and Fig. 4). These findings demonstrate the feasibility of reducing C_{max} and maintaining targeted displacement ratios. Finally, plots of displacement ratios as a function of C_{max}, $AUC_{0\text{-}\infty}$, or $AUC_{0\text{-}1.67\ h}$ of the drug exposure are shown in Fig. 5, A to C, respectively. $AUC_{0\text{-}1.67\ h}$ was specifically calculated because the TACs that delineated the [^{123}I]5-IA displacements mainly occurred within the first 100

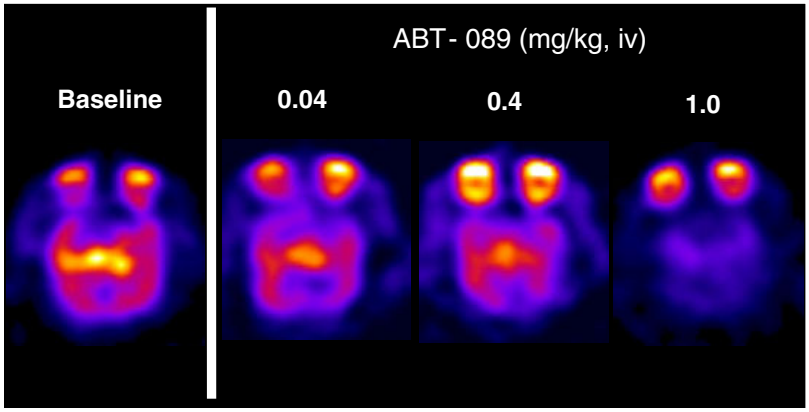

Fig. 3. Representative [^{123}I]5-IA SPECT images acquired at baseline and after ABT-089 infusion at various doses (0.04, 0.4, and 1 mg/kg i.v. slow infusion). It is noteworthy that displacement of tracer uptake at thalamus by ABT-089 infusion varied in a dose-related fashion.

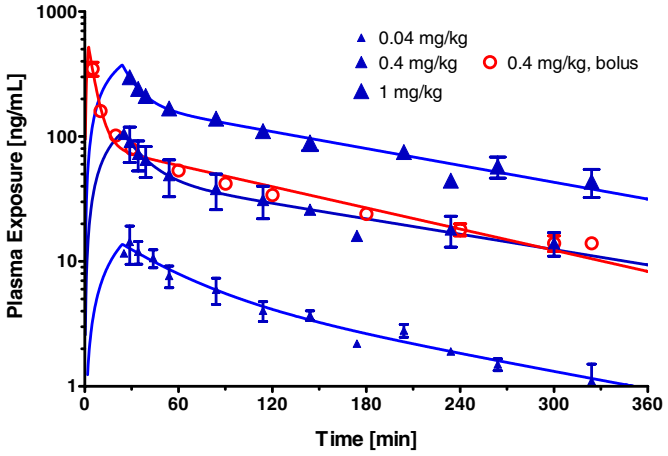

Fig. 4. Measured (mean ± S.E.M., symbols) and simulated (line) ABT-089 plasma concentration-time profiles at various doses (0.04, 0.4, and 1 mg/kg slow infusion and 0.4 mg/kg bolus injection). Pharmacokinetic simulation data were generated using the mean two-compartment model parameter estimates for each dose group.

min or 1.67 h after ABT-089 infusion (Fig. 1). The results indicate that, compared with C_{max}, displacement ratios can be better characterized by $AUC_{0-\infty}$ or $AUC_{0\text{-}1.67\ h}$ when a one-phase exponential association model is used. Thus, our data indicate that the displacement ratio is probably driven by the AUC of drug exposure, regardless of the dosing regimens used. Finally, a strong correlation ($R^2 = 0.97$, $p < 0.001$) was found between $AUC_{0-\infty}$ and $AUC_{0\text{-}1.67\ h}$ (Fig. 5D), suggesting that $AUC_{0\text{-}1.67\ h}$ can well represent $AUC_{0-\infty}$ and that AUC of plasma exposure beyond 1.67 h is essentially negligible.

Discussion

In this study, we examined the association between ABT-089 displacement ratios and plasma exposures in baboons using [^{123}I]5-IA SPECT imaging in which the dosing regimen was determined using two-compartment modeling with predetermined PK profiles. Our key finding is that similar displacement ratios were obtained for a given dose of ABT-089, regardless of whether the drug was given as a bolus injection or by slow infusion (Table 1). In particular, we showed that ABT-089 plasma exposures can be predicted by PK simulations, whereas the C_{max} can be established within a predetermined value (Fig. 2). Because the CNS-related adverse effects of nicotinic compounds are mainly driven by the C_{max} (Mansner and Mattila, 1977; Freeman et al., 1987), our data provide evidence that adverse effects can be potentially circumvented without compromising targeted binding activities.

In the past, PET imaging has been applied to determine the relationship between receptor binding and drug plasma exposure to drive dose selection for clinical studies (Farde et al., 1989; Movin-Osswald et al., 1994). For example, to study the PK profile of raclopride and its relationship with pharmacodynamic responses, Movin-Osswald et al. (1994) have previously examined the effect of administration rate on acathisia and prolactin. From their study, it was concluded that the frequency and duration of acathisia produced by raclopride seemed to mostly relate to plasma exposures, whereas the infusion rate was probably more correlated with the severity of symptoms. In fact, the high incidence of acathisia was associated with increased AUC of raclopride (Movin-Osswald et al., 1994). In light of the findings that acathisia is driven by high D_2-receptor occupancy (>80%) (Nyberg et al., 1995), our nAChR occupancy data are consistent with the previous findings that dopamine D_2-receptor binding activity is most probably determined by AUC instead of C_{max}. Nonetheless, in contrast to administering ascending doses infused over the same duration or the same dose administered over different rates, we determined the dosing regimen based on a two-compartment PK model that allows the adjustment of the dose and infusion times simultaneously. More importantly, the current approach can potentially be extended to predict the optimal oral-dosing regimens for human studies and thus facilitates the clinical development of novel therapeutics.

Previous radioligand binding studies have shown that ABT-089 interacts with high affinity at the $\alpha_4\beta_2$* subtype of both rodent and human nAChRs in which affinities were measured by displacement of specific [^{3}H](−)-cytisine binding from rat brain membranes (K_i = 17 nM) and from human $\alpha_4\beta_2$* nAChRs stably expressed in a human embryonic kidney cell line (Rueter et al., 2004). Results from our in vivo imaging study show that ABT-089 displaces [^{123}I]5-IA uptake at brain regions with a high density of $\alpha_4\beta_2$* nAChRs, which is consistent with these in vitro data. In contrast to in vitro studies, however, changes in the affinity state of receptors (Quick and Lester, 2002) or internalization may influence observed [^{123}I]5-IA binding patterns (Fujita et al., 2003a). ABT-089 has been shown to improve behavioral performance across a range of cognitive domains in animals (Decker et al., 1997) but has demonstrated a mixed picture of

TABLE 1
Calculated pharmacokinetic parameters and displacement ratios from the baboons administered with ABT-089 using different dosing regimens

Scan ID	ABT-089	Infusion Time	C_{max}	$AUC_{0-\infty}$	$AUC_{0\text{-}1.67\ h}$	Displacement
	mg/kg	*min*	*ng/ml*		*ng × h/ml*	*% baseline*
39	0.04	24	21	36	16	17.3
40	0.04	24	18	29	16	16.2
52	0.04	24	12	21	10	12.1
33	0.4	2	624	242	171	36.3
36	0.4	2	362	273	164	47.7
45	0.4	30	165	272	155	44.0
51	0.4	24	111	169	78	32.7
43	1.0	24	594	893	473	45.3
46	1.0	24	496	588	394	73.2
47	1.0	24	575	727	399	61.4

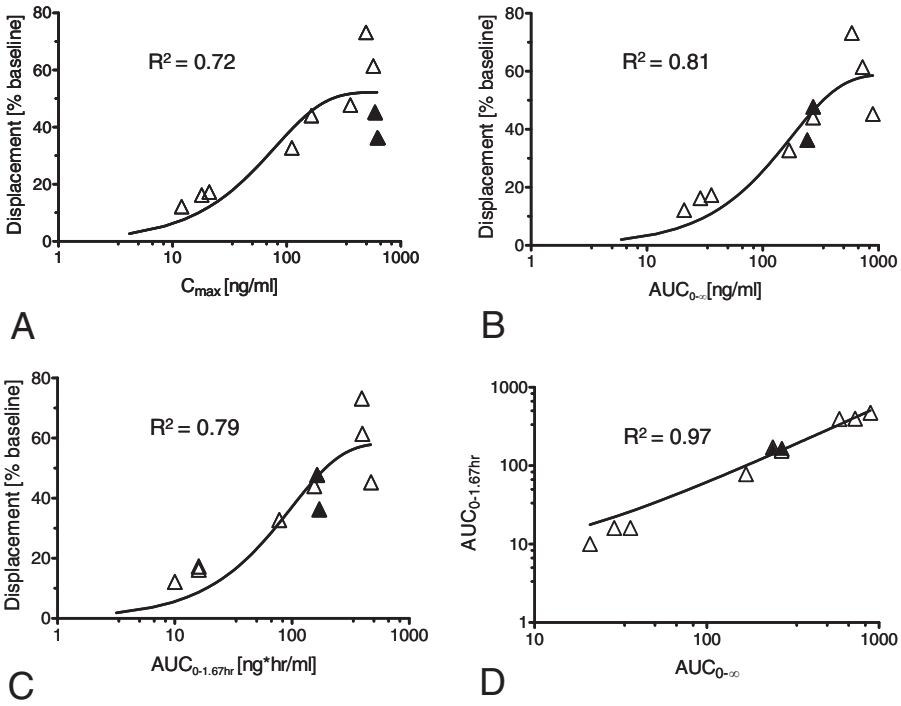

Fig. 5. Relationships between displacement ratios and ABT-089 plasma C_{max} (A), $AUC_{0-\infty}$ (B), or $AUC_{0\text{-}1.67\ h}$ (C) at different doses. The two filled triangles represent the baboon given a bolus injection of the drug (0.4 mg/kg i.v.). These data were fitted using the one-phase exponential association equation, and goodness of fit (R^2) was shown. It is noteworthy that strong correlation (R^2 = 0.97) was found between $AUC_{0-\infty}$ and $AUC_{0\text{-}1.67\ h}$ (D).

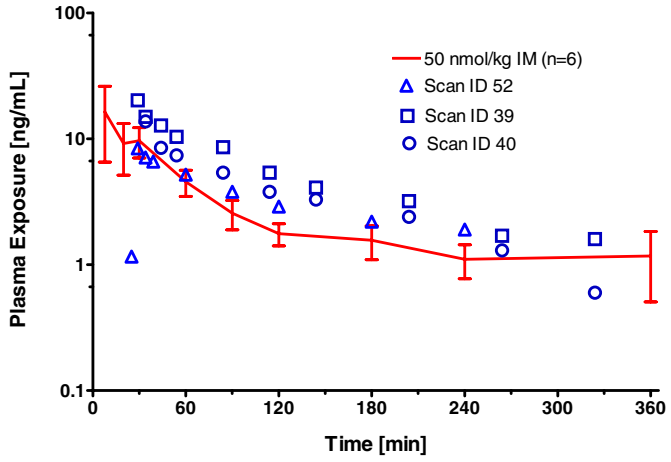

Fig. 6. Comparison of ABT-089 plasma concentration-time profiles achieved in our previous behavioral efficacy study (50 nmol/kg i.m., mean ± S.E.M., n = 6) (Decker et al., 1997) and the current imaging study (0.04 mg/kg i.v. slow infusion, symbols). As shown, similar exposure levels were observed between these experiments. Therefore, the displacement ratio-exposure relationship derived from the imaging study (Fig. 5) could potentially be used to guide dose selection for efficacy studies.

efficacy in humans (Wilens et al., 2006; Bain et al., 2009; Gault et al., 2009). One challenge to the development of compounds as ionotropic receptor agonists is the propensity for such compounds to demonstrate complex dose-response relationships. In the case of ABT-089, optimal efficacy on tasks such as delayed match to sample in primates is seen at peak exposures of 2 to 50 ng/ml and tends to diminish at higher exposures (Decker et al., 1997). Therefore, the standard approach of phase 2 dose selection of maximizing the dose based on phase 1 tolerability limits may not be optimal for a compound with this type of profile. For this reason, a translational receptor-occupancy study, with corresponding preclinical efficacy data, may assist in the evaluation of doses selected for clinical trials. For example, the lowest dose used in this study (0.04 mg/kg) was chosen to produce plasma exposures known to be efficacious in the delayed match-to-sample task in nonhuman primates (Fig. 6). Based on the exposure-receptor occupancy curve shown in Fig. 4, these exposures are expected to produce receptor occupancy of approximately 10 to 30%, which is substantially lower than those of needed to see efficacy with G protein-coupled receptor antagonists (e.g., >60-70% for D_2 antagonists). However, these findings are consistent with values obtained with other

agonists [e.g., ziprasidone at the $5HT_{1A}$ receptor (Grimwood and Hartig, 2009)]. This finding of behavioral efficacy with low receptor occupancy can be also reconciled with the steep dose-response curve observed for ABT-089 in primates (Prendergast et al., 1998), suggesting that receptor occupancies substantially beyond 20 to 30% do not provide additional cognitive efficacy and may diminish efficacy.

The relatively low occupancy required for the partial agonist ABT-089 in animal models contrasts with the much higher level of occupancy required for the D_2-partial agonist aripiprazole. Aripiprazole has been recently approved for treating psychiatric disorders and requires 90% receptor occupancy to achieve efficacy in preclinical animal models (Natesan et al., 2006) as well as in patients with schizophrenia (Gründer et al., 2008). Unlike other D_2-partial agonists that failed in clinical development, aripiprazole has high affinity for D_2/D_3 receptors and a long plasma half-life, which leads to high-receptor occupancy over a long period time (Gründer et al., 2008). The difference in receptor occupancy required for these two partial agonists is probably related to differences in the role of dopaminergic transmission in psychosis and nicotinic cholinergic transmission in cognitive function. Given the efficacy of D_2 antagonists in psychosis, the therapeutic action of aripiprazole in psychosis probably involves a partial agonist-induced reduction in dopaminergic transmission. In contrast, the cognitive effects of nAChR agonists are generally prevented by nAChR antagonists, suggesting that nAChR receptor activation is important for this action, although receptor desensitization may play a role in some therapeutic effects of nAChR agonists [e.g., antidepressant effects reported by Shytle et al. (2002)]. Indeed, an understanding of the dose/receptor-occupancy relationship is important in the interpretation of clinical trial data of drugs that act as receptor agonists, because the result can be dictated by intrinsic characteristics of the specific compound (e.g., affinity or plasma half-life).

In summary, PET and SPECT imaging can allow confirmation of brain penetration and target engagement and subsequently drive the dose selection for later clinical development; both imaging techniques have been increasingly exploited as a valuable tool for CNS drug discovery (Wong et al., 2009). In this work, by comparison of bolus and slow infusion dosing regimens, we demonstrated that displacement of [^{123}I]-5IA by ABT-089 is predominantly driven by the $AUC_{0\text{-}\infty}$ instead of the C_{max}. In conjunction with PK simulations, we showed that desired ABT-089 plasma exposure profiles can be established without diminishing targeted receptor occupancy levels. Because adverse effects of nicotinic agonists are mainly driven by the C_{max}, this observation indicates that a larger therapeutic window can be achieved through careful selection of dosing regimens, assuming that clinical efficacy is imparted by receptor binding in vivo.

Acknowledgments

We thank Drs. Chih-Hung Lee, Timothy Esbenshade, R. Scott Bitner, Robert Lenz, and Mario Saltarelli for insightful discussion.

Authorship Contributions

Participated in research design: Chin, Carr, Llano, Tamagnan, Decker, and Fox.

Conducted experiments: Barret and Xu.

Contributed new reagents or analytic tools: Xu, Koren, and Marsh.

Performed data analysis: Chin, Carr, Xu, Batis, Seibyl, and Tamagnan.

Wrote or contributed to the writing of the manuscript: Chin, Carr, Llano, Barret, Xu, Koren, Tamagnan, Decker, Day, and Fox.

References

Bain E, Apostol G, Sangal RB, Robieson WZ, Abi-Saab WM, and Saltarelli M (2009) Safety and efficacy of ABT-089, a novel α4β2 neuronal nicotinic receptor partial agonist, in the treatment of adults with attention-deficit/hyperactivity disorder, 56th Annual Meeting of the American Academy of Child and Adolescent Psychiatry, abstract 3.3; 2009 Oct 27–Nov 1; Honolulu, Hawaii. American Academy of Child and Adolescent Psychiatry, Washington, DC.

Baldwin RM, Zoghbi SS, Staley JK, Brenner E, Al-Tikriti MS, Amici L, Fujita M, Innis RB, and Tamagnan G (2006) Chemical fate of the nicotinic acetylcholinergic radiotracer [^{123}I]5-IA-85380 in baboon brain and plasma. *Nucl Med Biol* **33:**549–554.

Beleslin DB and Krstić SK (1987) Further studies on nicotine-induced emesis: nicotinic mediation in area postrema. *Physiol Behav* **39:**681–686.

Chefer SI, Horti AG, Lee KS, Koren AO, Jones DW, Gorey JG, Links JM, Mukhin AG, Weinberger DR, and London ED (1998) In vivo imaging of brain nicotinic acetylcholine receptors with 5-[123I]iodo-A-85380 using single photon emission computed tomography. *Life Sci* **63**:PL355–PL360.

Decker MW, Bannon AW, Curzon P, Gunther KL, Brioni JD, Holladay MW, Lin NH, Li Y, Daanen JF, Buccafusco JJ, et al. (1997) ABT-089 [2-methyl-3-(2-(*S*)-pyrrolidinylmethoxy)pyridine dihydrochloride]: II. A novel cholinergic channel modulator with effects on cognitive performance in rats and monkeys. *J Pharmacol Exp Ther* **283:**247–258.

Decker MW, Meyer MD, and Sullivan JP (2001) The therapeutic potential of nicotinic acetylcholine receptor agonists for pain control. *Expert Opin Investig Drugs* **10:**1819–1830.

Faessel HM, Gibbs MA, Clark DJ, Rohrbacher K, Stolar M, and Burstein AH (2006) Multiple-dose pharmacokinetics of the selective nicotinic receptor partial agonist, varenicline, in healthy smokers. *J Clin Pharmacol* **46:**1439–1448.

Farde L, Wiesel FA, Nilsson L, and Sedvall G (1989) The potential of positron-emission tomography for pharmacokinetic and pharmacodynamic studies of neuroleptics. *Psychopharmacol Ser* **7:**32–39.

Fox GB, Chin CL, Luo F, Day M, and Cox BF (2009) Translational neuroimaging of the CNS: novel pathways to drug development. *Mol Interv* **9:**302–313.

Frank R and Hargreaves R (2003) Clinical biomarkers in drug discovery and development. *Nat Rev Drug Discov* **2:**566–580.

Frankle WG and Laruelle M (2002) Neuroreceptor imaging in psychiatric disorders. *Ann Nucl Med* **16:**437–446.

Freeman GB, Sherman KA, and Gibson GE (1987) Locomotor activity as a predictor of times and dosages for studies of nicotine's neurochemical actions. *Pharmacol Biochem Behav* **26:**305–312.

Fujita M, Al-Tikriti MS, Tamagnan G, Zoghbi SS, Bozkurt A, Baldwin RM, and Innis RB (2003a) Influence of acetylcholine levels on the binding of a SPECT nicotinic acetylcholine receptor ligand [123I]5-I-A-85380. *Synapse* **48:**116–122.

Fujita M, Ichise M, van Dyck CH, Zoghbi SS, Tamagnan G, Mukhin AG, Bozkurt A, Seneca N, Tipre D, DeNucci CC, et al. (2003b) Quantification of nicotinic acetylcholine receptors in human brain using [^{123}I]5-I-A-85380 SPET. *Eur J Nucl Med Mol Imaging* **30:**1620–1629.

Fujita M, Tamagnan G, Zoghbi SS, Al-Tikriti MS, Baldwin RM, Seibyl JP, and Innis RB (2000) Measurement of alpha4beta2 nicotinic acetylcholine receptors with [123I]5-I-A-85380 SPECT. *J Nucl Med* **41:**1552–1560.

Gabrielsson JL and Weiner DL (1999) Methodology for pharmacokinetic/pharmacodynamic data analysis. *Pharm Sci Technolo Today* **2:**244–252.

Gault L, Apostol G, Wilens TE, Kratochvil CJ, Robieson WZ, Hall CM, Abi-Saab WM and Saltarelli M (2009) Safety and efficacy of ABT-089, a novel α4β2 neuronal nicotinic receptor partial agonist, in the treatment of children with attention-deficit/hyperactivity disorder, 56th Annual Meeting of the American Academy of Child and Adolescent Psychiatry, abstract 3.18; 2009 Oct 27–Nov 1; Honolulu, Hawaii. American Academy of Child and Adolescent Psychiatry, Washington, DC.

Gotti C and Clementi F (2004) Neuronal nicotinic receptors: from structure to pathology. *Prog Neurobiol* **74:**363–396.

Grimwood S and Hartig PR (2009) Target site occupancy: emerging generalizations from clinical and preclinical studies. *Pharmacol Ther* **122:**281–301.

Gründer G, Fellows C, Janouschek H, Veselinovic T, Boy C, Bröcheler A, Kirschbaum KM, Hellmann S, Spreckelmeyer KM, Hiemke C, et al. (2008) Brain and plasma pharmacokinetics of aripiprazole in patients with schizophrenia: an [18F]fallypride PET study. *Am J Psychiatry* **165:**988–995.

Hogg RC and Bertrand D (2007) Partial agonists as therapeutic agents at neuronal nicotinic acetylcholine receptors. *Biochem Pharmacol* **73:**459–468.

Horti AG, Koren AO, Lee KS, Mukhin AG, Vaupel DB, Kimes AS, Stratton M, and London ED (1999) Radiosynthesis and preliminary evaluation of 5-[$^{123/125}$I]iodo-3-(2(S)-azetidinylmethoxy)pyridine: a radioligand for nicotinic acetylcholine receptors. *Nucl Med Biol* **26:**175–182.

Howell LL (2008) Nonhuman primate neuroimaging and cocaine medication development. *Exp Clin Psychopharmacol* **16:**446–457.

Koren AO, Horti AG, Mukhin AG, Gündisch D, Kimes AS, Dannals RF, and London ED (1998) 2-, 5-, and 6-Halo-3-(2(S)-azetidinylmethoxy)pyridines: synthesis, affinity for nicotinic acetylcholine receptors, and molecular modeling. *J Med Chem* **41:**3690–3698.

Ludden TM, Beal SL, and Sheiner LB (1994) Comparison of the Akaike Information Criterion, the Schwarz criterion and the F test as guides to model selection. *J Pharmacokinet Biopharm* **22:**431–445.

Mansner R and Mattila MJ (1977) Pharmacokinetics of nicotine in adult and infant mice. *Med Biol* **55:**317–324.

Movin-Osswald G, Karlsson P, Hammarlund-Udenaes M, and Farde L (1994) Influence of rate of administration of raclopride on akathisia and prolactin response. *Psychopharmacology* (*Berl*) **114:**248–256.

Musachio JL, Villemagne VL, Scheffel UA, Dannals RF, Dogan AS, Yokoi F, and Wong DF (1999) Synthesis of an I-123 analog of A-85380 and preliminary SPECT imaging of nicotinic receptors in baboon. *Nucl Med Biol* **26:**201–207.

Natesan S, Reckless GE, Nobrega JN, Fletcher PJ, and Kapur S (2006) Dissociation between in vivo occupancy and functional antagonism of dopamine D2 receptors: comparing aripiprazole to other antipsychotics in animal models. *Neuropsychopharmacology* **31:**1854–1863.

Nyberg S, Nordstrom AL, Halldin C, and Farde L (1995) Positron emission tomography studies on D2 dopamine receptor occupancy and plasma antipsychotic drug levels in man. *Int Clin Psychopharmacol* **10 (Suppl 3):**81–85.

Paterson D and Nordberg A (2000) Neuronal nicotinic receptors in the human brain. *Prog Neurobiol* **61:**75–111.

Prendergast MA, Jackson WJ, Terry AV, Jr., Decker MW, Arneric SP, and Buccafusco JJ (1998) Central nicotinic receptor agonists ABT-418, ABT-089, and (−)-nicotine reduce distractibility in adult monkeys. *Psychopharmacology* (*Berl*) **136:** 50–58.

Quick MW and Lester RA (2002) Desensitization of neuronal nicotinic receptors. *J Neurobiol* **53:**457–478.

Rueter LE, Anderson DJ, Briggs CA, Donnelly-Roberts DL, Gintant GA, Gopalakrishnan M, Lin NH, Osinski MA, Reinhart GA, Buckley MJ, et al. (2004) ABT-089: pharmacological properties of a neuronal nicotinic acetylcholine receptor agonist for the potential treatment of cognitive disorders. *CNS Drug Rev* **10:**167–182.

Shytle RD, Silver AA, Lukas RJ, Newman MB, Sheehan DV, and Sanberg PR (2002) Nicotinic acetylcholine receptors as targets for antidepressants. *Mol Psychiatry* **7:**525–535.

Sullivan JP, Donnelly-Roberts D, Briggs CA, Anderson DJ, Gopalakrishnan M, Piattoni-Kaplan M, Campbell JE, McKenna DG, Molinari E, Hettinger AM, et al. (1996) A-85380 [3-(2(S)-azetidinylmethoxy) pyridine]: in vitro pharmacological properties of a novel, high affinity alpha 4 beta 2 nicotinic acetylcholine receptor ligand. *Neuropharmacology* **35:**725–734.

Wilens TE, Verlinden MH, Adler LA, Wozniak PJ, and West SA (2006) ABT-089, a neuronal nicotinic receptor partial agonist, for the treatment of attention-deficit/hyperactivity disorder in adults: results of a pilot study. *Biol Psychiatry* **59:**1065–1070.

Wong DF, Tauscher J, and Gründer G (2009) The role of imaging in proof of concept for CNS drug discovery and development. *Neuropsychopharmacology* **34:**187–203.

Zipursky RB, Meyer JH, and Verhoeff NP (2007) PET and SPECT imaging in psychiatric disorders. *Can J Psychiatry* **52:**146–157.

Zoghbi SS, Tamagnan G, Baldwin MF, Al-Tikriti MS, Amici L, Seibyl JP, and Innis RB (2001) Measurement of plasma metabolites of (*S*)-5-[^{123}I]iodo-3-(2-azetidinylmethoxy)pyridine (5-IA-85380), a nicotinic acetylcholine receptor imaging agent, in nonhuman primates. *Nucl Med Biol* **28:**91–96.

Address correspondence to: Dr. Chih-Liang Chin, Translational Imaging and Biochemical Biomarkers, Global Pharmaceutical Research and Development, Abbott Laboratories, Dept. R4DF, 100 Abbott Park Road, Bldg. AP4-2, Abbott Park, IL 60064. E-mail: chih-liang.chin@abbott.com